Nonlinear filamentation instability driven by an inhomogeneous current in a collisionless plasma

F. Califano,[1,2] R. Prandi,[1,3] F. Pegoraro,[1,4] and S. V. Bulanov[5]

[1]*Istituto Nazionale Fisica della Materia, Sezione A, Università di Pisa, Pisa, Italy*
[2]*Dipartimento di Astronomia, Università di Firenze, Firenze, Italy*
[3]*Dipartimento di Fisica Teorica, Università di Torino, Torino, Italy*
[4]*Dipartimento di Fisica, Università di Pisa, Pisa, Italy*
[5]*General Physics Institute, RAS, Moscow, Russia*

Beams of fast electrons in a cold electron background play a key role in the generation of a magnetic field in the wake of an ultrashort ultraintense laser pulse propagating in an underdense plasma. Here we study the linear and nonlinear evolution of the electromagnetic beam-plasma instability in a collisionless inhomogeneous plasma by using a set of two-fluid electron equations in the nonrelativistic and relativistic regimes. We show the characteristic spatial structures in the current and magnetic field distributions that are generated by this instability. These structures can be used as a signature of the physical mechanism at play in the analysis of the numerical and experimental results of the laser-plasma interaction. [S1063-651X(98)05412-9]

PACS number(s): 52.35.Qz, 52.35.Mw, 52.65.−y, 52.40.Nk

I. INTRODUCTION

Large-amplitude strongly nonlinear plasma waves may provide a very efficient mechanism for generating strong electron momentum anisotropies in plasmas as they produce beams of fast electrons. The currents associated with these fast electrons should give rise to very large magnetic fields which, however, are not observed at such high intensities either in laboratory experiments or in numerical simulations. This is due to the rapid reaction of the cold electron component present in the plasma which generates oppositely directed currents consisting of slow dense electron beams in order to maintain quasineutrality. The total net current in the plasma is then zero, but the free kinetic energy stored in the electron beams can now be partly converted into electromagnetic energy by means of beam-plasma instabilities. For perturbations perpendicular to the initial beam direction the relevant instability is the current filamentation (CF) instability [1–12]. This instability is similar to the Weibel instability [13] which occurs in a collisionless plasma with an anisotropic temperature. The CF instability is driven by the repulsion of the two oppositely directed currents which tends to reinforce any initial transverse perturbation. As a result, a magnetic field is generated and grows exponentially in time in the direction perpendicular to the wave vector of the perturbation and to that of the electron beams. This instability is electromagnetic with a purely imaginary frequency. In relativistic conditions, when the speed of the fast electron beam approaches the velocity of light, the CF instability is very efficient with a growth rate comparable to the electron-plasma frequency. Ions can thus be assumed to be immobile and to provide a uniform neutralizing background. In the case of strictly longitudinal perturbations, the excited mode is a purely electrostatic beam-plasma (BP) instability with a real and imaginary part of the frequency.

Particle in cell (PIC) numerical simulations [14–17] and, more recently, Vlasov-Maxwell simulations [18] of laser-plasma interactions have shown that quasistatic magnetic fields are generated in the wake of laser pulses. These mag-netic fields play a key role in the nonlinear dynamics of the plasma, and have important consequences regarding the energy transport and the pulse propagation and focalization. In these simulations [15,17,19,20] strong electron beams are generated at the breaking of the Langmuir wake plasma waves produced by the laser pulse. These beams are then thought to drive the instability responsible for the observed quasistatic magnetic fields. The spatial structure of the fields observed in the simulations is essentially dipolar and the magnetic field vanishes along the symmetry axis of the laser pulse propagation. In two-dimensional (2D) simulations of a linearly polarized laser pulse with its electric field directed perpendicular to the simulation plane, the quasistatic magnetic field is also perpendicular to this plane. In these simulations the spatial structure of the magnetic field, e.g., the number of different polarity domains, depends on the plasma and pulse parameters and evolves behind the pulse [19,20].

In the present paper we investigate the evolution of the electromagnetic beam-plasma (EMBP) instability, by which we denote the mode resulting from the coupling between the CF and BP instabilities. In the limit of two symmetric beams the BP instability is also known as the two-stream instability; see, e.g., [21] and [22]. We use a two-fluid electron approach with immobile ions. We consider a 2D inhomogeneous configuration with two initial counterstreaming electron beams localized in a finite width region with a width comparable to the electron skin depth. Such an initial configuration is relevant for the interpretation of the results of the PIC simulations. Our aim is to investigate the transition between different physical regimes and to identify the typical magnetic and current structures that can be used as characteristic signatures of the development of the EMBP instability and as markers of the different regimes, in the comparison with the numerical simulations of the laser-plasma interaction. Special attention is given to the case of strongly asymmetric beams, which is the most relevant in this comparison.

The formation of spatial structures due to the development of the CF instability, which we recall is analogous to the Weibel mode, was first reported for an inhomogeneous

plasma in [7], where it was shown both analytically and numerically that in a plasma with inhomogeneous beams the instability develops, already in its linear phase, a spatial ''resonant''-type singularity. This singularity occurs at the spatial location where the instability growth rate in the inhomogeneous configuration matches the growth rate, in the limit of large wave numbers, evaluated with the local values of the beam velocities. The largest magnetic field was found to be generated around this singularity and to have opposite polarities. In the case of transverse perturbations, a current layer was formed very rapidly at the resonance position, almost independent of the characteristic scale of the initial perturbation. On the other hand in a homogeneous plasma it was shown in [10,11] that, within the two-fluid description, transverse perturbations develop singularities in the electron beam densities and in the magnetic field in a finite time. These singularities correspond to compressional and/or rarefaction wave breaking and are due to a nonlinear energy cascade to smaller and smaller scales that, in a collisionless plasma in relativistic regime, is interrupted at the electron skin depth length scale by the kinetic effects considered in [10]. Again the magnetic field was found to be largest around these singularities and to have a dipolar structure.

This paper is organized as follows. In the next section we introduce the governing equations and the physical model used in this paper. In Sec. III we recall the main results concerning the linear evolution of two initial homogeneous and nonhomogeneous counterstreaming electron beams. In particular we show that in this phase the perturbations tend naturally to align themselves in the direction of the fast electron beam. This effect is strongest for relativistic beams. In Sec. IV we discuss the nonlinear inhomogeneous evolution and show that the spatial structures that are formed are essentially independent of the initial conditions on the perturbations. Conclusions follow in Sec. V.

II. THE TWO-FLUID ELECTRON EQUATIONS

In the linear phase and during the initial stage of the nonlinear phase, before the development of the resonant-type singularity and/or wave breaking during which the strong nonlinear interactions generate very small spatial scales, kinetic effects are negligible in the case of cold beams. Thus, before such scales are generated, we may study the evolution of two counterstreaming electron beams in the framework of the two-fluid electron equations where the ions are assumed to be at rest and to provide a uniform neutralizing background. This is consistent with the characteristic time of the development of the EMBP instability which, for velocities comparable to the speed of the light, is of the order of the inverse of the electron-plasma frequency. We recall that the role of kinetic effects in saturating the development of the CF instability and the formation of small scales was recently analyzed in [10] in the case of two homogeneous counterstreaming electron beams by numerically integrating the Vlasov-Maxwell equations.

We normalize all quantities by using a characteristic density $\bar{n}$, the speed of light c, and the electron-plasma frequency $\bar{\omega}_p = (4\pi\bar{n}e^2/m)^{1/2}$. Then, the dimensionless equations read

$$\frac{\partial n_a}{\partial t} = \nabla \cdot \mathbf{j}_a, \tag{1}$$

$$\frac{\partial \mathbf{p}_a}{\partial t} + \mathbf{v}_a \cdot \nabla \mathbf{p}_a = -(\mathbf{E} + \mathbf{v}_a \times \mathbf{B}), \tag{2}$$

$$\nabla \times \mathbf{B} = \frac{\partial \mathbf{E}}{\partial t} + \sum_a \mathbf{j}_a, \quad \nabla \cdot \mathbf{B} = 0, \tag{3}$$

$$\nabla \times \mathbf{E} = -\frac{\partial \mathbf{B}}{\partial t}, \quad \nabla \cdot \mathbf{E} = 1 - \sum_a n_a, \tag{4}$$

where

$$\mathbf{v}_a = \frac{\mathbf{p}_a}{(1 + p_a^2)^{1/2}}, \quad \mathbf{j}_a = -n_a \mathbf{v}_a, \quad a = 1,2.$$

Notice that the normalized electron skin depth is equal to 1.

At the initial time the two electron beams are directed in opposite directions along the x axis and are localized in the central region around the $y = 0$ point,

$$\mathbf{v}_{0,1} = v_{0,1}\cosh^{-2}(y/l)\mathbf{e}_x, \quad \mathbf{v}_{0,2} = -\mathbf{v}_{0,1}n_{0,1}/n_{0,2}, \tag{5}$$

where $n_{0,1} + n_{0,2} = 1$ and the initial total net current is zero, $n_{0,1}v_{0,1} + n_{0,2}v_{0,2} = 0$. For the sake of simplicity, in the following we assume that the initial densities are homogeneous; i.e., $n_{0,1}(t=0), n_{0,2}(t=0)$ do not depend on x and y. In Eq. (5) the subscript zero refers to zero-order (equilibrium) quantities and l is the typical width of the beams. This equation models the two initially interpenetrating currents discussed in the Introduction: the current of the fast electrons generated by the breaking of plasma wake waves and the denser return current carried by the cold plasma.

We limit our analysis to a magnetic field with a single component parallel to the z axis, $\mathbf{B} = (B_z)$, while the electric field $\mathbf{E} = (E_x, E_y)$ and the electron momenta $\mathbf{p}_a = (p_{0,a} + p_{a,x}, p_{a,y})$ are in the x-y plane.

III. LINEAR REGIME

First we recall some analytical results on the evolution of small disturbances before nonlinear interactions due to the growth of the unstable modes become important. Relativistic effects are explicitly taken into account.

A. Homogeneous beams

In the ''ideal'' case of two homogeneous electron beams, corresponding to $l \to \infty$ in Eq. (5), and of periodic disturbances of the form

$$f(x,y,t) \sim e^{i(k_x x + k_y y - \omega t)}, \tag{6}$$

the dispersion relation of the counterstreaming instability can be derived analytically [7] (see also [22]) by solving the algebraic system obtained by linearizing Eqs. (1)–(4):

$$(1 - \Omega_2^{-2})[k_x^2(1 + \Omega_4^{-2}) - \omega^2(1 - \Omega_1^{-2}) - 2\omega k_x \Omega_3^{-2}]$$
$$+ k_y^2[(1 - \Omega_1^{-2})(1 + \Omega_4^{-2}) + \Omega_3^{-4}] = 0, \tag{7}$$
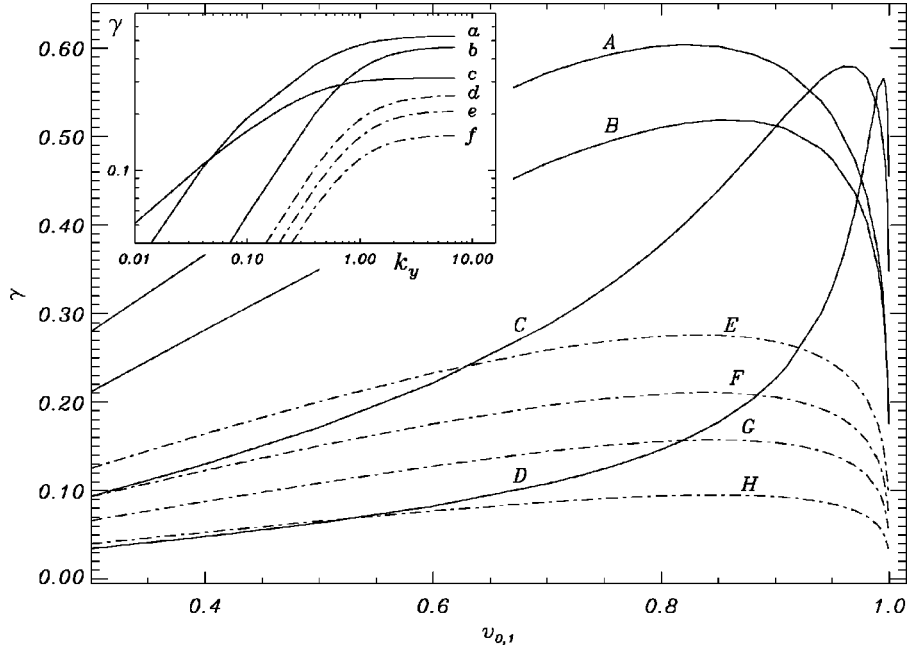
FIG. 1. The growth rate of the CF instability, $k_x=0$, vs $v_{0,1}$ and, top left corner, vs k_y. The solid lines refer to the symmetric case $n_{0,1}=n_{0,2}=0.5$ dot-dashed lines to the nonsymmetric case $n_{0,1}=0.167$ and $n_{0,2}=0.833$. Curves C,D,G,H are multiplied by 3, 11, 5, 30, respectively. The parameters of all the curves are given in Table I.

where

$$\Omega_1^{-2}=\sum_a \frac{n_{0,a}}{\Gamma_a\Omega_a^2}, \quad \Omega_2^{-2}=\sum_a \frac{n_{0,a}}{\Gamma_a^3\Omega_a^2},$$

$$\Omega_3^{-2}=\sum_a \frac{n_{0,a}v_{0,a}}{\Gamma_a\Omega_a^2}, \quad \Omega_4^{-2}=\sum_a \frac{n_{0,a}v_{0,a}^2}{\Gamma_a\Omega_a^2}, \quad (8)$$

and $\Omega_a=\omega-k_x v_{0,a}$, $\Gamma_a=(1-v_{0,a}^2)^{-1/2}$. Notice that Eq. (7) is fully general since, as remarked in Ref. [7], in a nonmagnetized, homogeneous plasma there are only two preferential directions, that of the electron beams and that of the wave vector of the perturbation.

Equation (7) describes electromagnetic or purely electrostatic modes depending on the angle between the perturbation wave vector and the stream direction, i.e., depending on the values of k_x and k_y. We notice that in Eq. (7) the solution is invariant with respect to the sign of k_y and to the sign of the pair (ω, k_x), where $\omega=\omega_r+i\gamma$ is the mode complex frequency, but in general not with respect to the signs of ω and of k_x independently. Since $(k_y,k_x,\omega_r,\gamma)$ and $(-k_y, -k_x,-\omega_r,\gamma)$ label the same mode, Eq. (7) describes modes with a dispersion relation that depends on their direction of propagation (on the sign of their phase velocity) along the x axis, while their frequency and growth rate are independent of the sign of ω/k_y. In addition growing and damped modes appear in pairs with the same value of $|\gamma|$. When $k_x=0$ and, for arbitrary k_x, in the special symmetric case where $v_{0,1}=-v_{0,2}$, Eq. (7) is quadratic in ω and leads to purely growing instabilities or to purely oscillatory modes.

1. One-dimensional dispersion relation

When the wave vector is parallel to the electron beams, $k_y=0$, the BP instability amplifies the longitudinal electric

field E_x with a growth rate obtained by solving the equation $1-\Omega_2^{-2}=0$. No magnetic field is produced in this case. In the opposite limit, $k_x=0$, the dispersion relation (7) (see also [6]) reduces to

$$\omega^6-(\hat{\Omega}_1^2+\hat{\Omega}_2^2+k_y^2)\omega^4-[k_y^2(\hat{\Omega}_4^2-\hat{\Omega}_1^2)-\hat{\Omega}_1^2\hat{\Omega}_2^2]\omega^2$$
$$+k_y^2(\hat{\Omega}_1^2\hat{\Omega}_4^2-\hat{\Omega}_3^4)=0, \quad (9)$$

where $\hat{\Omega}_j^2\equiv\omega^2\Omega_j^{-2}$ with Ω_j^{-2} defined by Eq. (8) with $k_x=0$. Equation (9) contains two oscillatory solutions and one purely growing mode which corresponds to the CF instabil-

TABLE I. Physical parameters of the results shown in Fig. 1.

Curve	$n_{0,1}$	$n_{0,2}$	k_y
A	0.5	0.5	3.14
B	0.5	0.5	1.0
C	0.5	0.5	0.1
D	0.5	0.5	0.01
E	0.167	0.833	3.14
F	0.167	0.833	1.0
G	0.167	0.833	0.1
H	0.167	0.833	0.01
Curve	$n_{0,1}$	$n_{0,2}$	$v_{0,1}$
a	0.5	0.5	0.95
b	0.5	0.5	0.5
c	0.5	0.5	0.995
d	0.167	0.833	0.95
e	0.167	0.833	0.5
f	0.167	0.833	0.995

ity and generates a magnetic field B_z perpendicular to the plane (x,y) of the electron streams and of the wave vector of the perturbation.

In Fig. 1 we plot the growth rate γ of the CF instability, $k_x = 0$, vs the beam velocity $v_{0,1}$ and, in the top left corner, vs the transversal wave number k_y. In both figures the solid lines refer to the symmetric case $n_{0,1} = n_{0,2} = 0.5$, while dot-dashed lines refer to the nonsymmetric case $n_{0,1} = 0.167$ and $n_{0,2} = 0.833$. The parameters are given in Table I. For reasons of presentation, curves C, D, G, H, which correspond to small values of k_y and thus to small values of γ, are multiplied by the numerical factors 3,11,5,30, respectively.

We note that in both the symmetric and nonsymmetric cases the growth rates increases with the beam velocity $v_{0,1}$, reaches a maximum, and then decreases in the relativistic regime due to the increase of the effective electron mass. In the symmetric case (equal beam densities and opposite velocities) the position of the maximum moves towards larger values of the beam velocity as the wave number decreases, curves A-D. On the other hand, in the nonsymmetric case the position of the maximum and the qualitative behavior of the growth rate depend only weakly on the wave number, curves E-H. In Sec. III B we will see that the nonmonotonic behavior of the growth rate has important consequences regarding the development of the CF instability in the inhomogeneous case.

As it is well known, the growth rate of the CF instability (curves a-b-c-d-e-f) increases linearly with the wave number k_y in the small wave number case (long wavelength), $k_y \ll 1$, and saturates in the large wave number limit (small wavelength), $k_y \gg 1$. Of importance for the following analysis is the fact that in the nonsymmetric case, curves d-e-f, the critical wave number at which the growth rate of the CF instability saturates, k_{crit}, remains unchanged going from the nonrelativistic to the relativistic regime. On the other hand, as discussed in Ref. [7], in the symmetric relativistic case, curves a-b-c, the instability growth rate saturates at lower and lower values of k_y, an effect due to the relativistic increase of the effective electron skin depth. The saturation of the growth rate with respect to the wave number at $k_y \equiv k_{crit}$ is relevant to the development of the instability in the 1D inhomogeneous case where, as mentioned in the Introduction, the characteristic spatial scale of the growing mode is generated by a resonant mechanism. As discussed in Ref. [7], the characteristic wave number $k_y \equiv k_{res}$ of the growing resonant mode is fixed by the value at which the growth rate saturates, $k_{res} \simeq k_{crit}$, regardless of the wave number k_{0y} of the initial perturbation (assuming $k_{0y} < k_{crit}$). In addition, in 2D, the value of the wave number of the resonant mode, $k_{res} \simeq k_{crit}$, determines not only the value of the growth rate, but also the nature of the mode since whether the instability is dominated by the CF or by the BP instability depends on the angle between the resulting wave number and the electron beams, i.e., the ratio between k_y and k_x.

If the initial beams are symmetric, then $\hat{\Omega}_3^2 = 0$, and one of the two oscillatory solutions of Eq. (9) reduces to purely electrostatic Langmuir waves decoupled from the two other branches. In this limit the CF growth rate is given by

$$\gamma = \frac{1}{\sqrt{2}} \left\{ \left[\sqrt{\left(\frac{1}{\Gamma^3} + k_y^2 \right)^2 + \frac{4 k_y^2 v_0^2}{\Gamma}} - \left(\frac{1}{\Gamma^3} + k_y^2 \right) \right] \right\}^{1/2}. \tag{10}$$

In the nonrelativistic regime $\Gamma = 1$, Eq. (10) can be reduced, in the small and large wave number limits, to the well-known expressions

$$\gamma_s \sim |v_0| k_y, \quad k_y \ll 1, \tag{11}$$

$$\gamma_l \sim |v_0|, \quad k_y \gg 1, \tag{12}$$

in agreement with the main features observed in Fig. 1. By requiring $\gamma_s \sim \gamma_l$, we obtain the value of k_y beyond which the growth rate saturates, $k_y = k_{crit} \sim 1$, or in dimensional units, $\tilde{k}_{crit} \sim 1/d_e$. In the relativistic limit $|v_0| \approx 1$, Eq. (10) can be reduced, in the small, intermediate, and large wave number limit, to

$$\gamma_s \sim |v_0| \Gamma k_y, \quad k_y < 1/\Gamma^{5/2}, \tag{13}$$

$$\gamma_i \sim (|v_0| k_y / \Gamma^{1/2})^{1/2}, \quad 1 > k_y > 1/\Gamma^{5/2}, \tag{14}$$

$$\gamma_l \sim |v_0| \Gamma^{-1/2}, \quad k_y > 1, \tag{15}$$

in agreement with the results of Fig. 1. An intermediate region appears between the small wave number and the saturated, large wave number regions, characterized by a sublinear slope. This intermediate interval is clearly shown by curve c where a linear increase of the growth rate with k_y only occurs for very small wave numbers. The growth rate dependence on the Lorentz factor Γ changes from γ_s to γ_l in agreement with Fig. 1, curves a-c, where we see that γ increases monotonically with $v_{0,1}$ in the small wave number limit, while in the opposite case the maximum growth rate (curve a) does not correspond to the maximum beam velocity (curve c). The transition from the γ_s regime to the γ_i and γ_l regime is also shown by curves A-D where we see that the increasing and decreasing regions of the growth rate vs $v_{0,1}$ strongly depend on the wave number.

By requiring $\gamma_i \sim \gamma_l$ we obtain, in agreement with Fig. 1, that in the relativistic regime the value of k_y beyond which the growth rate saturates becomes lower and lower, $k_{crit} \sim v_0 \Gamma^{-1/2}$ (we recall that $|v_0| \approx 1$), an effect due to the relativistic increase of the effective electron skin depth. The different behavior observed in the nonsymmetric case (see Fig. 1, curves d,e,f), where k_{crit} is independent of the beam velocity, can be explained as follows. When the initial beams are nonsymmetric, $n_{0,1} \ll n_{0,2}$, $v_{0,1} \gg v_{0,2}$, and the fast one is relativistic, $|v_{0,1}| \approx 1$, $\Gamma_2 \sim 1$ and $\Gamma_1 = \Gamma \gg 1$, we can expand the coefficients in Eq. (9) in powers of $n_{0,1}$ and obtain, to leading order,

$$\hat{\Omega}_1^2 \approx \hat{\Omega}_2^2 \approx 1, \quad \hat{\Omega}_3^4 \approx n_{0,1}^2 v_{0,1}^2, \quad \hat{\Omega}_4^2 \approx n_{0,1} v_{0,1}(v_{0,1}/\Gamma - v_{0,2}). \tag{16}$$

Then, to leading order, the growth rate is given by

$$\omega^2 \approx - \frac{k_y^2 n_{0,1} v_{0,1}^2}{(1 + k_y^2) \Gamma}, \tag{17}$$

from which we obtain the following asymptotic behaviors of the homogeneous CF instability for strongly nonsymmetric initial beams:

$$\gamma_s \sim (n_{0,1} v_{0,1}^2 / \Gamma)^{1/2} k_y, \quad k_y \ll 1, \tag{18}$$
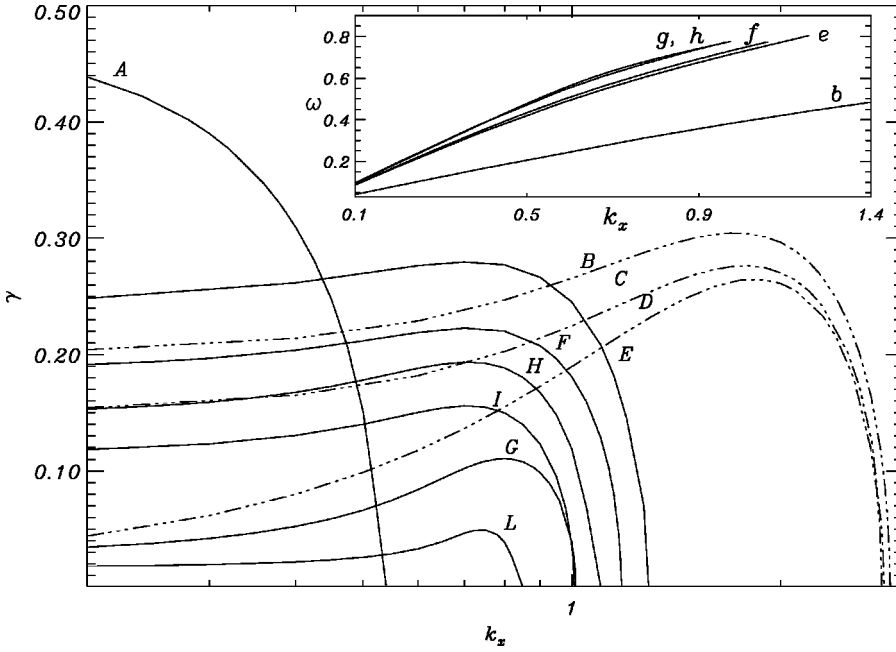
FIG. 2. The growth rate of the EMBP instability and, top right corner, its frequency vs k_x. The solid lines refer to the relativistic case, and the dot-dashed lines to the nonrelativistic case. The parameters of all the curves are given in Table II.

$$\gamma_l \sim (n_{0,1}v_{0,1}^2/\Gamma)^{1/2}, \quad k_y \gg 1, \qquad (19)$$

where $v_{0,1} \approx 1$.

By requiring $\gamma_s \sim \gamma_l$, we find that the value of k_y beyond which the growth rate saturates, $k_y = k_{\text{crit}} \sim 1$, is independent of the beam initial velocity, in agreement with the result shown in Fig. 1.

These different scalings of the saturation of the CF growth rate with respect to the wave number k_y derived in this section will determine how the characteristic width of the current channels and of the magnetic field generated by the instability depend on the properties of the accelerated electron beam and of the return current.

2. Two-dimensional dispersion relation

In the general case when both k_x and k_y are different from zero, the CF instability and the BP instability are part of a single branch which we denote as the EMBP instability.

In Fig. 2 we plot the growth rate of the EMBP instability vs k_x for different values of k_y. The parameters are given in Table II. Curves A and E–L are relativistic and curves B–D nonrelativistic. Curve A corresponds to the symmetric case; all others are nonsymmetric. Finally, curves B-E-H are obtained for a transverse wave vector k_y larger than in the other cases. In the top right corner we plot the frequency of the instability, curves b-e-f-g-h, with the same parameters of the corresponding curve in capital letters.

In general, except for the symmetric ($n_{0,1} = n_{0,2}$) relativistic case shown by curve A, the maximum growth rate is reached when the wave vector forms an angle with the direction of the beams different from 0 and $\pi/2$, i.e., for $k_y \neq 0$ and $k_x \neq 0$. We observe that the value of k_x of the most unstable mode is practically independent of k_y for a given value of the beam velocity $v_{0,1}$ and that the most unstable mode, curves B-E-H, occurs at values of k_x smaller than k_y, i.e., at $k_x < k_y$. Furthermore, the angle between the wave vector of the most unstable mode and the direction of the electron beams decreases significantly for increasing values

of the beam velocity $v_{0,1}$. Thus we can expect that in the relativistic regime the CF instability dominates with respect to the BP; i.e., the typical magnetic structures become more and more homogeneous in the stream direction. This is easily understood by noticing that the dispersion relation of the BP instability shows that only the long wavelength modes, i.e., modes with small k_x, are unstable. In the homogeneous symmetric case, $n_{0,1} = n_{0,2}$, the BP instability condition gives

$$k_x v_0 < \Gamma^{-3/2}, \qquad (20)$$

which becomes more and more stringent as relativistic conditions are approached. A similar argument holds in the nonsymmetric case. However, Fig. 2 shows that the relativistic stabilization of the BP instability is more effective in the symmetric case, curve A, than in the nonsymmetric case, curves E–G. By comparing curves E,F,G with curves

TABLE II. Physical parameters of the results shown in Fig. 2.

Curve	$n_{0,1}$	$n_{0,2}$	$v_{0,1}$	k_y
A	0.5	0.5	0.95	1.0
B	0.167	0.833	0.5	3.14
C	0.167	0.833	0.5	1.0
D	0.167	0.833	0.5	0.1
E	0.167	0.833	0.95	3.14
F	0.167	0.833	0.95	1.0
G	0.167	0.833	0.95	0.1
H	0.167	0.833	0.995	3.14
I	0.167	0.833	0.995	1.0
L	0.167	0.833	0.995	0.1
Curve	$n_{0,1}$	$n_{0,2}$	$v_{0,1}$	k_y
b	0.167	0.833	0.5	3.14
e	0.167	0.833	0.95	3.14
f	0.167	0.833	0.95	1.0
g	0.167	0.833	0.95	0.1
h	0.167	0.833	0.995	3.14

H,I,L, we see that, regardless of the transversal wave number k_y, the growth rate in the relativistic limit decreases for increasing velocities (at least for velocities greater than a critical value), as we have already noticed for the ''pure'' CF instability. We conclude that the CF instability dominates with respect to the BP instability in the relativistic regime, which implies that the typical magnetic structures become more and more homogeneous in the stream direction.

B. Nonhomogeneous beams

In the laser-plasma simulations the electron beams generated by the laser pulse are concentrated in a central region of finite width which is represented in our model by the parameter l in Eq. (5). Here we limit our investigation to electron beams with typical width somewhat larger than the plasma electron skin depth and take $l=4$. This choice is consistent with the values of the laser pulse width used in the simulations of the laser plasma interaction (see, e.g., [15–17,20]).

In the numerical integration of the fluid equations (1)–(4), we have used periodic boundary conditions in the direction of the electron streams, along the x axis, and free-slip boundary conditions $\partial/\partial y = 0$, in the transverse direction, along the y axis. The numerical mesh is non-uniform in the transverse direction with a refined grid in the central region. The typical time step and grid space are $0.001 \leqslant dt \leqslant 0.01$, $dx \simeq 0.025$, and $dy \simeq 0.01$ (dy is calculated in the inhomogeneous region). A detailed discussion of the numerical code can be found in [7] (see also [24] for details on the numerical algorithm).

At the initial time we introduce a ''small'' magnetic perturbation

$$B_z = \epsilon R(x,y) \exp[-y^2/(2\sigma^2)], \quad (21)$$

where ϵ is the amplitude of the initial perturbation and $R(x,y) \exp[-y^2/(2\sigma^2)]$ represents its spatial distribution with a typical transversal width σ.

1. One-dimensional evolution

Let us first consider the pure 1D CF case $k_x = 0$. By expressing all quantities in the form $F(y,t) = f(y)e^{\gamma t}$, the linearized system of equations (1)–(4) can be cast into a second-order differential equation for the inductive electric field E_x:

$$\frac{\partial}{\partial y}\left[f(v_{0,1/2}(y),\gamma^2)\frac{\partial E_x}{\partial y}\right] - g(v_{0,1/2}(y),\gamma^2)E_x = 0, \quad (22)$$

where

$$f(v_{0,1/2},\gamma^2) = \gamma^2 + \frac{\hat{\Omega}_3^4}{(\gamma^2 + \hat{\Omega}_1^2)} - \hat{\Omega}_4^2,$$

$$g(v_{0,1/2},\gamma^2) = \gamma^2(\gamma^2 + \hat{\Omega}_2^2), \quad (23)$$

and the coefficients $\hat{\Omega}_i$ are defined below Eq. (9). A local Frobenius analysis [23] analogous to the one performed in [7] for the nonrelativistic case shows that the solution of Eq. (22) is singular at the points $\bar{y}$ where $f(v_{0,1/2}(\bar{y}),\gamma^2) = 0$. At

these points the coefficient of the second-order derivative vanishes. In a homogeneous plasma, $f(v_{0,1/2}(\bar{y}),\gamma^2) = 0$ gives the instability growth rate in the limit $k_y \to \infty$. We notice that in the nonrelativistic symmetric limit $f(v_{0,1/2},\gamma^2)$ reduces to $\gamma^2 - v_0(y)^2$, in agreement with [7] [here $v_0(y) = v_{0,1} = -v_{0,2}$].

In the case of an even equilibrium such as the one given by Eq. (5), two symmetric resonant points $\pm\bar{y}$ are present in the nonrelativistic case. As a consequence, regardless of the initial wavelength, the perturbation is rapidly concentrated in the inhomogeneous region between the two singularities. In order to find the position of the singularities in the relativistic case, i.e., the solutions of $f(v_{0,1/2}(\bar{y}),\gamma^2) = 0$, we consider, for example, the case of two nonsymmetric, relativistic beams, $n_{0,1} = 1/6$, $n_{0,2} = 5/6$, and $v_{0,1} = 0.95$, and use as an ansatz a value of the growth rate close to that obtained from the corresponding 1D homogeneous case for large values of k_y. Then, $f(v_{0,1/2}(\bar{y}),\gamma_{inh}^2) = 0$ shows the presence of four singular points, symmetrically located with respect to $y=0$. This doubling of the resonance condition is a direct consequence of the nonmonotonicity of the growth rate with respect to the beam velocity in the relativistic regime discussed in Sec. III A 1. Looking at Fig. 1 (curves $A-H$), it is clear that the condition $f(v_{0,1/2},\gamma^2) = 0$ at fixed γ^2 is in general satisfied by two different values of $v_{0,1}$, one of them relativistic (and by the two corresponding values of $v_{0,2}$). Since in the inhomogeneous case the initial beam is formed of electrons with different velocities decreasing outwards, we expect that in the relativistic regime there exist two distinct resonant points on each side of the beam. The external resonance involves slower and ''lighter'' electrons and the internal one fully relativistic ''heavier'' electrons. Thus, when the electron beams are relativistic ($v_{0,1} \geqslant 0.95$), the resulting structure is characterized by two layers on each side of the beam, each layer being similar to the one observed in the presence of nonrelativistic beams ($v_{0,1} = 0.5$).

In order to investigate the role of the resonance on the growth rate and on the resulting currents and magnetic field structure in detail, we performed a number of 1D runs in the interval $-30 \leqslant y \leqslant 30$, taking $\sigma = 7.07$, $R(y) = \sin(k_{0y}y + \phi)$ in Eq. (21), while varying the most relevant physical parameters, $0.5 \leqslant v_0 \leqslant 0.995$, $0.01 \leqslant k_{0y} \leqslant 1$, and $0 \leqslant \phi \leqslant \pi$. As described in [7], the ''resonant'' CF mode is rapidly excited with a growth rate independent of the initial wave number k_{0y} and of the initial phase ϕ of the perturbation. Therefore, after the initial (rapid) transient, all the modes with the same beam velocities grow with the same growth rate.

In Fig. 3 we show the results of four nonsymmetric runs, $n_{0,1}/n_{0,2} = 0.2$, before nonlinear effects take place modifying the structure of the resonant mode. In the first three frames (A)-(B)-(C), we plot the current j_x vs y in the nonrelativistic case, $v_{0,1} = 0.5$, for three different values of the phase ϕ. In the last frame (D), we plot the same quantity in the relativistic case, $v_{0,1} = 0.95$. In the linear nonrelativistic regime the current structure depends on the initial phase of the perturbation, while it is completely independent in the relativistic regime (this latter conclusion is supported by a number of runs not presented here). Figure 3 shows that in the nonrelativistic case the current (as well as the magnetic and electric fields) is characterized by a single layer central structure,
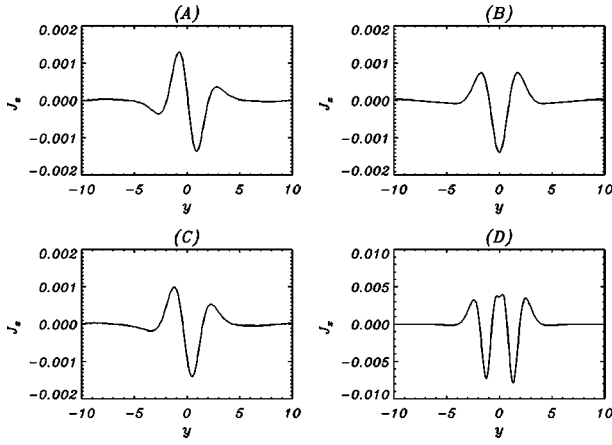
FIG. 3. The total current in the stream direction in the linear phase for three non-relativistic runs, $v_{0,1}=0.5$ $[(A)-(B)-(C)]$ with different initial phases, $\phi=0, \pi/2, \pi/4$, respectively, and a relativistic run, $v_{0,1}=0.95$ $[(D)]$. All these runs are nonsymmetric, $n_{0,1}/n_{0,2}=0.2$.

located between the two singular points, and that this layer doubles in the relativistic case. This doubling of the current structure is in agreement with the previous analytical study of the resonance condition, which shows that the number of the singular points doubles in the relativistic limit. We notice that this doubling of the layer structure is a general result in the relativistic regime, as confirmed by a large number of simulations, not presented here, for a wide range of parameters, $0.95 \leq v_{0,1} \leq 0.9995$, $0.5 \leq n_{0,1}/n_{0,2} \leq 0.1$, and $0.1 \leq k_{0y} \leq 1$.

2. Two-dimensional evolution

We integrate the system of equations (1)–(4) in the intervals $0 \leq x \leq 2\pi$, $-30 \leq y \leq 30$ with $\sigma=7.07$ and $R(x,y) = \sin(0.3y) \Sigma_k \sin(kx+\phi_k)$, $k=0, \ldots, 8$, in Eq. (21).

In this case where both k_x and k_y in the initial perturbation are different from zero, the CF instability is coupled to the BP instability; we denote the coupled mode as the EMBP instability. As discussed in Sec. III A, the BP instability amplifies the longitudinal electric field E_x in the beam direction for a limited range of long wavelength modes. In the relativistic regime, the smallest unstable wavelength becomes increasingly large, as shown by Eq. (20). The characteristic dimensionless length scale of this instability is $l_{ts} \simeq v \Gamma^{3/2}$. No magnetic field is produced in this case.

The competition between the CF instability, which tends to separate the currents in the transverse y direction, and the BP instability, which tends to modulate the currents in the longitudinal x directions, is shown in Fig. 4 where we plot the isocontours of the magnetic field and of the longitudinal electric field in two nonsymmetric cases: the first is nonrelativistic and the second is relativistic. This figure shows the linear stage of the EMBP instability during the exponential growth after the resonant mechanism has taken place. As in the 1D case, the resonance rapidly pinches the initial perturbation to typical wave vectors comparable to those of the most unstable 2D homogeneous mode, both in the nonrelativistic $k_x \simeq 1.7$, $k_y = \pi$ and in the relativistic $k_x \simeq 0.7$, $k_y = \pi$, cases (curves B and E in Fig. 2). As a result, the growth
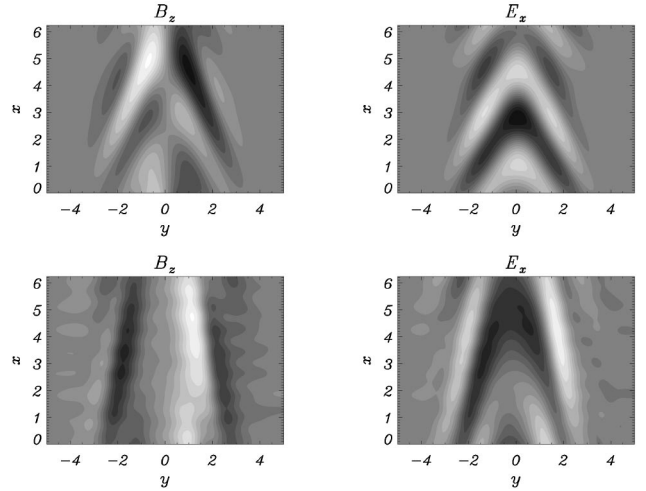
FIG. 4. The isocontours of the magnetic field B_z and of the longitudinal electric field E_x during the linear phase in the nonrelativistic case, $v_{0,1}=0.5$, $n_{0,1}=0.167$, $n_{0,21}=0.833$, first two frames, and in the relativistic case, $v_{0,1}=0.95$, $n_{0,1}=0.167$, $n_{0,21}=0.833$, last two frames.

rate also becomes of the order of the growth rate of the most unstable 2D homogeneous mode.

In the nonrelativistic regime the EMBP instability is spatially characterized by a transversal dipolar magnetic field with an arrowlike structure which becomes almost aligned in the stream direction in the relativistic regime, as expected by the linear homogeneous analysis, Sec. III A. This mode becomes completely aligned in the stream direction in the pure symmetric relativistic case (not shown here).

In the last two frames of Fig. 4 we see the characteristic two-layer dipolar magnetic structure already observed in the 1D pure CF case as consistent with the fact that the CF instability dominates the 2D relativistic regime.

IV. NONLINEAR EVOLUTION

In Sec. III B we have discussed the linear evolution of the EMBP instability in the inhomogeneous case. We have seen that the wavelength of the initial perturbation is rapidly reduced by the resonant mechanism to typical lengths of the order of the electron skin depth, regardless of its initial value. Then, the perturbation amplitude is amplified with a growth rate of the order of the maximum growth rate in a homogeneous plasma as obtained by solving Eq. (7). In this linear phase, the structure of the current and of the magnetic field depends, in the nonrelativistic case, on the initial conditions and, in particular, on the initial phase. However, as soon as nonlinear interactions become important, the formation in a finite time of singularities related to wave breaking, as mentioned in the Introduction, strongly modifies the shape of the perturbations (see also [10,11]).

This is illustrated in the 1D cases in Fig. 5 where we show the behavior in the nonlinear phase of the same quantities shown in Fig. 3 in the linear phase. The comparison of these two figures shows that in all nonrelativistic cases the resulting current system is now characterized by the presence of a central ''fast'' current with two ''slow'' return currents on both sides. Therefore, the system becomes practically independent of the initial conditions, even if the spatial location
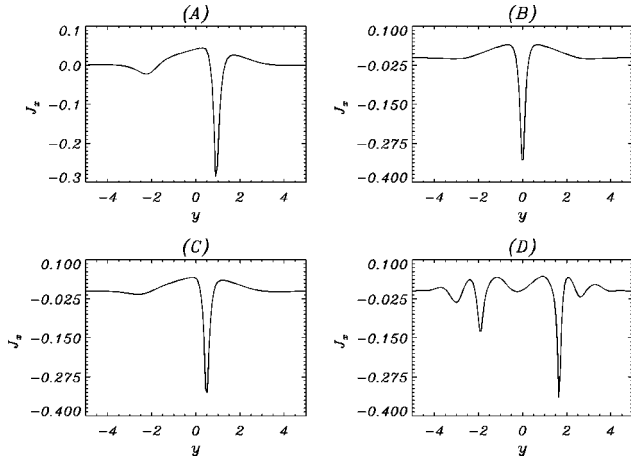
FIG. 5. The total current in the stream direction in the nonlinear phase for three nonrelativistic runs, $v_{0,1}=0.5[(A)\text{-}(B)\text{-}(C)]$ with different initial phases, $\phi=0,\pi/2,\pi/4$, respectively, and a relativistic run, $v_{0,1}=0.95[(D)]$, $\phi=0$. All these runs are nonsymmetric, $n_{0,1}/n_{0,2}=0.2$.

of the fast central beam depends slightly on the initial phase ϕ of the perturbation. In the relativistic nonlinear case, as in the linear case, the resulting current system does not depend on the initial conditions (this is seen in a number of simulations not presented here). Notice that the presence of a two-layer structure in the relativistic limit still holds in the nonlinear regime.

The 2D nonlinear phase is illustrated by Figs. 6 and 7 which show the magnetic field, the transverse electric field (perpendicular to the beam direction), and the densities in the nonlinear regime for a nonrelativistic and for a relativistic simulation, respectively. The main effect observed in the nonlinear regime is a transverse wave break which pinches all the physical quantities in the y direction. Since the plasma is assumed to be collisionless, this effect leads to the formation of smaller and smaller scales $k_y \gg k_y^{\mathrm{res}}$, well below the electron skin depth (see also [11]) This nonlinear pinching is a pure transverse effect, so that the typical structures remain
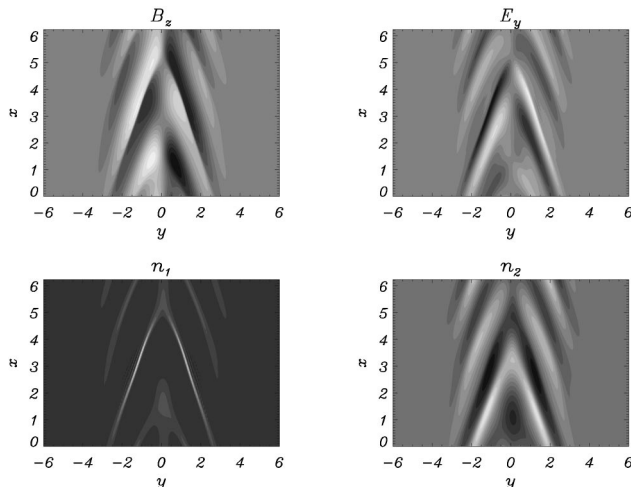
FIG. 6. The isocontours of the magnetic field B_z, of the electric field E_y transversal to the beams, and of the densities n_1 and n_2 in a nonsymmetric, $n_{0,1}=0.167$, $n_{0,2}=0.833$, nonrelativistic, $v_{0,1}=0.5$, case.
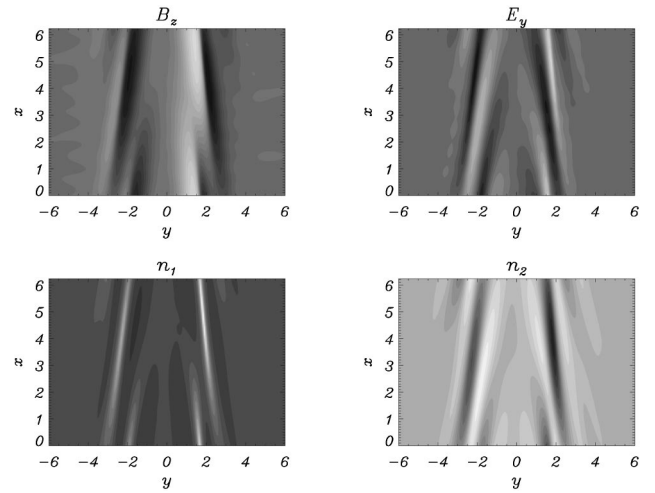
FIG. 7. The isocontours of the magnetic field B_z, of the electric field E_y transversal to the beams, and of the densities n_1 and n_2 in a nonsymmetric, $n_{0,1}=0.167$, $n_{0,2}=0.833$, relativistic, $v_{0,1}=0.95$, case.

essentially those generated by the linear resonant mechanism, even if much thinner (see Fig. 4 for a comparison). Another effect, that is also observed in the 1D case, is the generation of a strong electrostatic field. In the nonrelativistic case this field is comparable to the magnetic term in the Lorentz force and in the relativistic regime it even dominates. We recall that the electrostatic field is negligible during the linear regime. Again, we notice that in the nonlinear regime, the nonrelativistic EMBP instability is still characterized by a modulated structure in the beam direction. It becomes more and more homogeneous in the relativistic case with a double magnetic dipole structure.

The large gradients observed in Figs. 6 and 7 in the y direction will change, on longer time scales, the plasma dynamics, due to the setup of kinetic effects.

V. CONCLUSIONS

Magnetic field generation is a fundamental process in plasma physics and astrophysics since it provides a very efficient mechanism for transferring and storing free kinetic energy into magnetic energy which can then be abruptly released on fast time scales by some mechanism, as, for example, magnetic reconnection. In this process the plasma dynamics, its transport properties, etc., can be completely modified and new strong nonlinear magnetic interactions come into play.

In recent years, self-induced, ultrastrong quasistatic magnetic fields have been observed in numerical experiments involving the interaction of large amplitude, ''relativistically'' strong, laser pulses with plasmas. These fields play a fundamental role in the dynamics of the wake fields generated by the laser pulse as shown, e.g., in an underdense plasma in [17]. Instabilities due to beams of counterstreaming electrons were invoked [14,15] in order to explain the buildup of magnetic energy, since fast electron streams can be easily generated in relativistic regimes by the breaking of plasma waves. In this paper, using a relativistic two-fluid approach, we have studied the linear and nonlinear evolution

of the EMBP instability in conditions that are directly relevant for the laser plasma interactions. In particular we have assumed that the initial electron streams are concentrated in a narrow region corresponding to the finite transverse dimension of the laser pulse.

In the nonrelativistic linear case, the resulting current structure depends on the initial conditions and in particular on the phase of the perturbation. This is no longer true in the nonlinear regime where wave breaking generates the same structure regardless of the initial conditions. This structure is characterized by a central ''fast'' current and two ''slow'' return currents with an arrowlike shape in the stream direction. On the other hand, in the relativistic case the currents are independent of the initial conditions even during the linear phase and are practically homogeneous in the stream direction. A double current layer is formed already in the linear stage. A quasistatic dipolar magnetic field is observed both in the nonrelativistic and relativistic regimes. In the relativistic regime a doubling of the dipole magnetic field structure is observed. These results are in very good agreement with the results obtained in PIC simulations [19,20] and support the conclusion that the current structure and the magnetic field observed in the wake of a ''relativistically strong'' laser-pulse impinging on a underdense plasma are generated by the development of the EMBP-type instability. We may speculate that in the full 3D case secondary instabilities fed by the magnetic shear generated by the instability will develop and lead to a full 3D dynamics and/or to collisionless magnetic reconnection events. However, this regime will be characterized by the presence of a strong nonlinear interaction and by the presence of very small spatial scales, where kinetic effects cannot be neglected.

The work presented here is motivated by the attempt to identify characteristic magnetic and current structures produced by the EMBP instability which can be then used in order to recognize typical signatures of this physical process in laser-plasma experiments. This comparison has proved successful as shown in [19,20]. However, it should be observed that the occurrence of singularities leading to very small spatial scales cannot be fully described with the fluid approximation adopted in this paper. A kinetic description that properly describes this phase is for the moment available only for the case of a homogeneous plasma [10]. An extension of the present work to the full nonlinear kinetic regime after the formation of the singularities is in progress by numerical integration of the Vlasov-Maxwell equations.

[1] G. Kalman, C. Montes, and D. Quemada, Phys. Fluids **11**, 1797 (1968).

[2] N.W. Albright, Phys. Fluids **13**, 1021 (1970).

[3] R.L. Morse and W. Nielson, Phys. Fluids **14**, 830 (1971).

[4] R.C. Davidson, D.A. Hammer, I. Haber, and C.E. Wagner, Phys. Fluids **15**, 317 (1972).

[5] V.Yu. Bychenkov *et al.*, Zh. Éksp. Teor. Fiz. **98**, 1269 (1990) [Sov. Phys. JETP **71**, 79 (1990)].

[6] F. Pegoraro, S.V. Bulanov, F. Califano, and M. Lontano, Phys. Scr. **T63**, 262 (1996).

[7] F. Califano, F. Pegoraro, and S.V. Bulanov, Phys. Rev. E **56**, 963 (1997).

[8] F. Califano, F. Pegoraro, and S.V. Bulanov, *Europhysics Conference Abstracts*, 24th European Conference on Controlled Fusion and Plasma Physics, Berchtesgaden, Germany, 1997, Vol. 21A, p. 1329.

[9] F. Califano, R. Prandi, F. Pegoraro, and S.V. Bulanov, in *Superstrong Fields in Plasma*, Proceedings of the First International Conference on Superstrong Fields in Plasmas, AIP Conf. Proc. No. 426, edited by M. Lontano, G. Mourou, F. Pegoraro, and E. Sindoni (AIP, New York, 1998).

[10] F. Califano, F. Pegoraro, S.V. Bulanov, and A. Mangeney, Phys. Rev. E **57**, 7048 (1998).

[11] F. Califano, R. Prandi, F. Pegoraro, and S.V. Bulanov, J. Plasma Phys. (to be published).

[12] Y. Kazimura, F. Califano, J. Sakai, T. Neubert, F. Pegoraro, and S.V. Bulanov, J. Phys. Soc. Jpn. **67**, 1079 (1998).

[13] E. Weibel, Phys. Rev. Lett. **2**, 83 (1959).

[14] D.W. Forslund and J.M. Kindel, Phys. Rev. Lett. **54**, 558 (1985).

[15] G.A. Askar'yan, S.V. Bulanov, F. Pegoraro, and A.M. Pukhov, JETP Lett. **60**, 241 (1994).

[16] G.A. Askar'yan, S.V. Bulanov, F. Pegoraro, and A.M. Pukhov, Comments Plasma Phys. Control. Fusion **10**, 173 (1995).

[17] S.V. Bulanov, T.Zh. Esirkepov, M. Lontano, F. Pegoraro, and A.M. Pukhov, Phys. Rev. Lett. **76**, 3562 (1996).

[18] H. Ruhl, Jpn. J. Appl. Phys. (to be published).

[19] F. Pegoraro, S.V. Bulanov, F. Califano, T. Liseikina, A. Mangeney, N. Naumova, and V. Vshivkov, Electromagnet. Waves and Electron. Syst. (to be published).

[20] S.V. Bulanov, F. Califano, T. Liseikina, F. Pegoraro, and V. Vshivkov (unpublished).

[21] N. Krall and A. Trivelpiece, *Principles of Plasma Physics* (McGraw-Hill, New York, 1978), p. 478.

[22] A. Alexandrov, L. Bogdankevich, and A. Rukhadze, *Principles of Plasma Electrodynamics* (Springer-Verlag, Berlin, 1984), p. 167.

[23] C.M. Bender and S.A. Orszag, *Advanced Mathematical Methods for Scientist and Engineering* (McGraw-Hill, New York, 1978), p. 70.

[24] F. Califano, Comput. Phys. Commun. **99**, 29 (1996).